Force Production Mechanisms for a Flat Plate Wing at Low Reynolds Numbers (Invited)

Simon Corkery* and Holger Babinsky†

Department of Engineering, University of Cambridge, United Kingdom

Micro Air Vehicles (MAVs) operate in highly unsteady and often separated flow conditions which are well outside the usual design space of conventional lifting surfaces. This paper aims to coalesce theory and simply explain the physical mechanisms behind force production for such unsteady and separated flows with regards to added mass and circulatory (vortex dynamics) effects. Particle Image Velocimetry (PIV) and flow visualisation are additionally used to show that the 'non-circulatory' added mass forces are responsible for production of vorticity bound to the wing surface, thus can be confused with free vortices in the flow field. Changes to the 'added mass vorticity' and thus forces derived from this are shown to be independent of flow topology and perhaps viscous effects in general with exception to edge conditions. A technique to simply quantify the distribution of the bound vorticity from PIV measurements is additionally described and utilised.

I. Introduction

Micro air vehicles are small, portable, covert and manoeuvrable unmanned aircraft that can be fitted with optical, acoustic, or chemical sensors. The devices can therefore find application in tasks including military surveillance, search and rescue, or chemical monitoring in both hazardous or inaccessible environments. Some designs of MAVs take inspiration from successful low Reynolds biological fliers such as birds and insects and utilise flapping wings to produce lift, whist others follow the more conventional fixed wing and multi-rotor aircraft designs. A unifying design issue between each configuration is that the aerodynamic lifting surfaces can be required to operate under highly unsteady aerodynamic conditions, whether that is caused by the kinematic motion of the aerofoil itself, or by the high levels of atmospheric turbulence. Atmospheric turbulence can be of the same order of magnitude as the MAVs flight speed, thus wind conditions that larger aircraft are impervious to can cause significant flight instability to MAVs. Under such conditions flow about the lifting surfaces is typically dominated by regions of flow separation at the leading and trailing wing edges, which can amalgamate into large leading and trailing edge vortices. For both the purpose of MAV design, or for utilisation on an onboard flight controller for pre-emptive disturbance rejection, it is desirable to understand the mechanisms responsible for force generation on wings subjected to such large unsteady aerodynamic conditions.

This paper aims to present a simple deconstruction of the total force on a flat plate wing into 'circulatory' and 'non-circulatory' components, which explain the process of lift generation from a phenomenological perspective. Bisplinghoff et al.[1] describes circulatory and non-circulatory flows as those with and without their attendant lines or sheets of vortices respectively. While this definition is useful, it will later be discussed why it is difficult to classify real flows in such a clear cut manner. As a result some models which have based force components from PIV measurements of a flow field have 'double counted' non-circulatory effects.[2,3]

Hereafter the paper will proceed by describing the forces on a flat plate wing in planar motion, followed with a description of the unifying link between circulatory and non-circulatory force components. This is followed by the methodology and results of flow visualisation and PIV experiments on a linearly and rotationally

*Ph.D., sjc276@cam.ac.uk.

†Professor, hb@eng.cam.ac.uk, AIAA Associate Fellow.

accelerated wing. Each of the experiments are designed to place emphasis on how the non-circulatory forces are made visible in a viscous flow field and how they can be quantified with PIV measurement.

II. Force components for a flat plate in 2D planar motion

For simplicity the analysis of force components will be limited to an infinitely thin flat plate and the flow field is assumed to be two dimensional, incompressible and irrotational. Although flow about real aircraft is inherently three dimensional in nature, it has been shown that three-dimensional effects take relatively long time periods to develop in comparison to the unsteady motions described here.[2] For modelling purposes the flow field can therefore be assumed to be two-dimensional. Most of the flow field is assumed to be inviscid, however viscous effects are included in the model by concentrating vorticity into singular point and sheet vortices that reside 'outside' of the otherwise inviscid flow field. This approach is taken to enable the computation of circulatory force components, while maintaining the simplicity and insight attained with potential models.

Under these assumptions the flow field can be described by potential flow models based on Milne-Thomson's[4] circle theory. The complex potential ($f(\zeta) = \phi + i\psi$) given by Eldredge and Wang,[5] as well as Michelin and Llewellyn Smith[6] for a flat plate wing (with chord length c) undergoing arbitrary planar motion in the presence of n point vortices is,

$$f(\zeta) = \overbrace{\underbrace{-\frac{iU_n c/2}{\zeta}}_{\text{translation}} \underbrace{-\frac{i\Omega(c/2)^2/4}{\zeta^2}}_{\text{rotation}}}^{\text{non-circulatory}} + \overbrace{\sum_{j=1}^{n} \frac{\Gamma_j}{2\pi i}\left(\underbrace{\log(\zeta-\zeta_j)}_{\text{shed circ.}} - \underbrace{\log(\zeta-\zeta_{j,m})}_{\text{mirror/bound circ.}}\right)}^{\text{circulatory}}. \quad (1)$$

A more complete exposition can be found in papers by Eldredge and Wang[5] or Michelin and Llewellyn Smith,[6] so only a brief description of each variable is given here. The variable U_n is the plate velocity component in the direction normal to the surface, while Ω is the angular velocity of the plate in the anticlockwise direction. Γ_j is the circulation for point vortices $j = 1$ to n in the flow field. The complex variable $\zeta = \epsilon + i\eta$ is the location of a reference point in a mapped (circle) plane that is used to determine the flat plate solution. The circle plane is related to the physical plate co-ordinate frame of reference ($z = x + iy$) by the mapping relation $z = c(\zeta + \frac{1}{\zeta})$. For every vortex in the flow field there must be a 'mirror' vortex to both satisfy the no penetration condition through the plate surface and conservation of circulation. The mirror vortex is located at $\zeta_{j,m}$, which is related to the 'parent' free vortex by $\zeta_{j,m} = 1/\zeta_j^*$, where ζ_j^* is the complex conjugate of ζ_j. The first pair of terms in equation (1), which are illustrated in figure 1, are the non-circulatory components. This comprises a part due to translation of the plate in the surface normal direction and a component due to rotation about the mid chord location. The second pair of terms in equation (1) are the circulatory components. The circulatory components arise due to the external vortices in the flow field and the corresponding mirror vortices that give rise to bound circulation on the plate. The means which the non-circulatory and circulatory terms contribute to a force on the plate is discussed next.

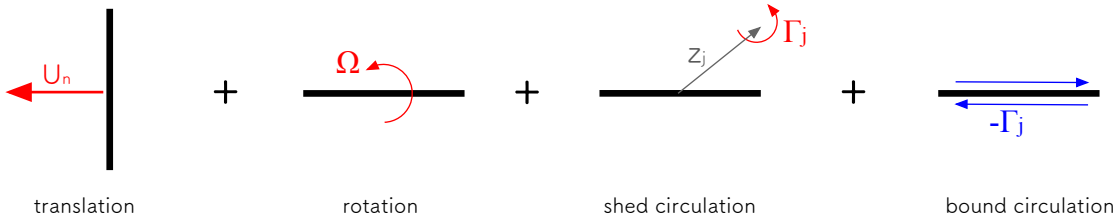

Figure 1: Components that contribute to the total force response of a flat plate wing

A. Non-circulatory forces: Added mass

The non-circulatory force components arise through enforcing the no-penetration condition on the plate in an inviscid flow field. Figures 2a and 2b show the translation and rotation only components of the stream-function given by equation 1 respectively. Each plot is shown for the frame of reference of a plate moving through an initially quiescent fluid, thus appear different to the conventional potential flow streamline pattern for flow streaming past a stationary plate. Since the streamlines intersect the surface of the plate and due to the no-penetration condition, fluid elements adjacent to the plate must travel with the plate. Due to continuity, particles 'away' from the plate must also be displaced to make way for the moving plate. As a result the whole flow field must have some finite motion and thus kinetic energy. If the plate is travelling at constant velocity, this kinetic energy is constant and thus there can be no net work done and therefore no net force on the plate. If the speed of the plate were to change, so would the flow velocity. The kinetic energy of the fluid would thus be changed, therefore work is done on the fluid and a net force must have been applied (by the plate and to the flow field and vice versa). Because the flow field is inviscid and incompressible, the force applied to the fluid must be actioned by pressure waves that emanate instantaneously from the plate surface.

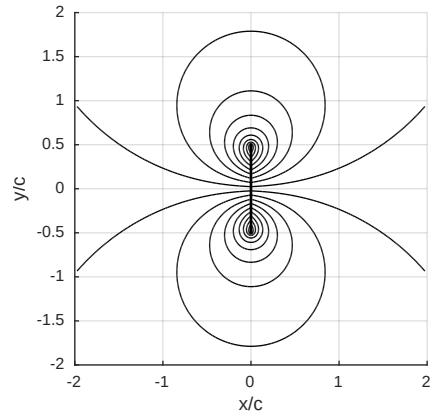

(a) Translation: $\alpha = 90°$

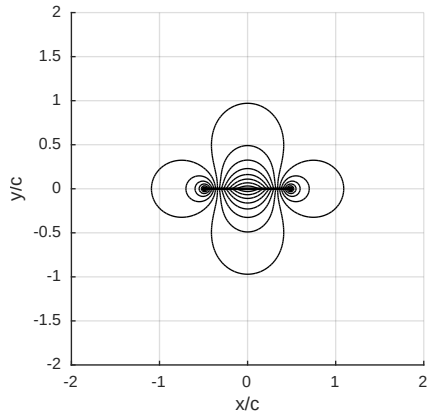

(b) Rotation: $\alpha = 0°$

Figure 2: Streamlines for a translating and rotating plate in inviscid fluid. Frame of reference is for a stationary fluid at infinity.

If now we consider the frame of reference for flow streaming past a fixed plate, the velocity of any fluid element in the flow field for a wing translating in the normal direction with velocity $U_n(t)$ is

$$u(z,t) = K(z)U_n(t), \tag{2}$$

where K(z) is a position variant scaling factor.[7] The net fluid momentum in the plate normal direction, per unit length is

$$J_n(z,t) = U_n(t)\rho\Big|\int_A K(z)dA\Big|. \tag{3}$$

The force on the plate in the direction opposite the acceleration vector is equal to the rate of change of momentum, therefore

$$F_n = \frac{\partial J_n}{\partial t} \tag{4}$$

$$= \underbrace{\rho\Big|\int_A K(z)dA\Big|}_{\text{added mass}} \overbrace{\dot{U}_n}^{\text{accel.}}, \tag{5}$$

where the integral term is the added mass of fluid. The added mass term is not the total mass of fluid in the flow field (which can extend to infinity), rather it represents simply the mass of a finite, albeit non-physical volume of fluid travelling at the plate velocity, with equivalent momentum to that of the full flow field. For the plate shown in figure 2a the added mass is equivalent to $\rho\pi c^2/4$, the mass of a cylindrical volume of fluid with diameter equal to one chord and unit length. For the rotating plate shown in figure 2b the added mass is zero in the x-y directions, but is instead replaced with a finite added 'mass moment of inertia' that resists angular acceleration.

B. Circulatory forces: Production and advection of vortices

As shown in figure 3a the flow field surrounding a flat plate wing can be dominated by large flow separation, that can form a leading and trailing edge vortex (LEV and TEV respectively). The effect of these vortices is modelled by the circulatory terms in equation (1). If at first we assume all vorticity is contained in singular leading and trailing edge point vortices, the flow field would look similar to that of the inviscid vortex pair shown in figure 3b. Lamb[8] showed that the flow field about a pair of equal and opposite inviscid point vortices has net momentum (J_n), in the direction normal to a line of length d between the vortex centres.

$$J_n = \rho\Gamma d \tag{6}$$

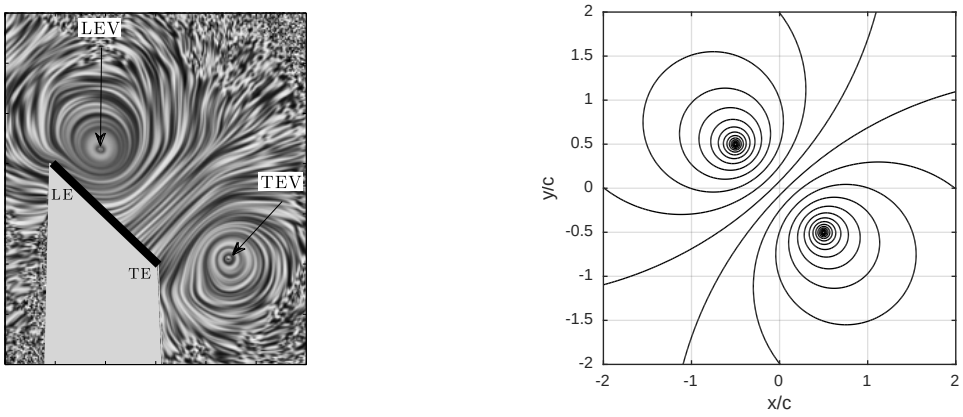

(a) Impulsively accelerated flat plate wing.[9]

(b) Point vortex model

Figure 3: Representation of a LEV and TEV as a pair of equal and opposite point vortices.

As force is time rate of change of momentum, equation (7) shows that a force must be applied to the fluid if the pair of point vortices were to either grow in strength ($\dot{\Gamma} \neq 0$), or advect relative to one another ($\dot{d} \neq 0$). Physically this force must have been applied to the flow field by the plate.

$$F_n = \rho(\underbrace{\dot{\Gamma} d}_{\text{growth}} + \underbrace{\dot{d}\Gamma}_{\text{advection}}) \tag{7}$$

While Lamb derived the momentum for a vortex pair, the result can be generalised for an arbitrary vorticity distribution in a flow field. As Kelvin's theorem states that circulation is conserved, every element of circulation in a flow field must have a complementary opposite element elsewhere. The total momentum of the flow field can thus be found by summation of each of the vortex element pairs. We can thus obtain the general result given by Wu,[10]

$$J_x = \rho \int_A y\omega dA \qquad\qquad J_y = \rho \int_A x\omega dA, \tag{8}$$

where ω is vorticity and dA an elemental area (note, $d\Gamma = \omega dA$). For each element of circulation generated by a body, the 'equal and opposite' vortex resides as bound circulation on the body, as required to satisfy conservation of circulation and the no-penetration condition. In an inviscid flow this bound circulation resides 'inside' the body surface, however, in a real viscous flow the circulation is contained in the viscous boundary layer surrounding the body. These ideas can be seen by considering the starting flow for an impulsively accelerated wing. Vorticity is shed from the trailing edge to satisfy the Kutta condition, while the mirror vorticity resides in the boundary layer on the wing surface. At steady state the lift force of the wing can be explained by equation (7), as there is finite rate of change of distance between the starting and bound vortices ($\dot{d} \neq 0$), while at steady state the Γ is constant. We therefore obtain the Kutta-Joukowski result $L = -\rho U_\infty \Gamma$, where $U_\infty = \dot{d}$. Equally, the drag force on a bluff body can be attributed to the finite rate at which vorticity is shed into a flow field. If at steady state the boundary layers either side of the body separate at finite distance (d), the drag force on the body is equal to the growth term of equation (7).

Equation 8 states that the total momentum of the flow field (and therefore force) can be found with knowledge of the circulation and distribution of all vortex elements. This at first appears to conflict with the description of non-circulatory forces described in section A, for which a force was derived seemingly without requiring vorticity. This is addressed next.

C. The link between circulatory and non-circulatory force components

While the force due to added mass is often referred to as non-circulatory, it is not truely independent of vorticity production. In inviscid theory a body in a flow field is represented by making a streamline equivalent to the body surface, thereby enforcing the no penetration condition. While the streamline can be constructed by a number of means, one convenient method represents the body as a vortex sheet. In this approach, the sheet strength is given by equation (9) and is equivalent to the vorticity contained in a boundary layer when taken to the Euler limit.[11,12] This is a convenient approach which bridges the gap between inviscid and viscous perspectives of a flow field, because boundary layer vorticity in a viscous flow field (at infinite Reynolds number) is represented. The approach does, however, require modification in cases of flow separation.

$$\gamma = u_2 - u_1 \tag{9}$$

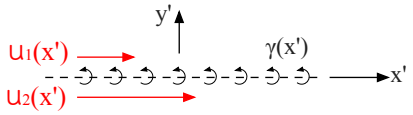

Figure 4: Vortex sheet representation of surface vorticity

The velocity components u_1 and u_2 of equation (9) can be found from the complex potential given by equation (1) and thus the strength of the vortex sheet for a plate undergoing any arbitrary planar motion, with an arbitrary number of vortices in the flow field can be found. So now, if we use the 'free vortices' to represent any shed vorticity due to flow separation, this model can represent a separated viscous flow. Furthermore, the free vortices do not specifically have to be generated by the plate at all. The equations are equally valid for vortices generated in the flow field by other aerofoils, or even wind gusts which can also be represented by a series of vortex elements. The general plate vortex sheet equation is,

$$\gamma_{plate} = \underbrace{-2U_n \frac{x'}{\sqrt{(c/2)^2 - x'^2}}}_{\text{translation}} \underbrace{- \Omega \frac{2x'^2 - (c/2)^2}{\sqrt{(c/2)^2 - x'^2}}}_{\text{rotation}} \underbrace{- \sum_{j=1}^{n} \frac{\Gamma_j}{\pi \sqrt{(c/2)^2 - x'^2}} \frac{\zeta_j^2 - 1}{\zeta_j^2 - 4\zeta_j \frac{x'}{c} + 1}}_{\text{free vortices}}, \tag{10}$$

where x' is the distance from the centre of the plate tangential to the surface. Immediately we see that there is a component of the vortex sheet that is proportional to the plate normal velocity U_n and the angular velocity Ω. If we take just the translation component, circulation elements can be attained from equation (10) ($d\Gamma = \gamma dx'$) and thus from equation (8) we have the net momentum of the flow field. The

net momentum is proportional to U_n, thus the net force is proportional to $\dot{U}_n$. The net force attained is equivalent to the 'non-circulatory' added mass force given previously in section A. A variation of equation (10) has additionally been used by Graham et al.,[13] who showed that with knowledge of the plate kinematics and PIV measurements of the starting vortex, the impulse due to the bound vortex sheet can be determined. The authors successfully matched the force as calculated from flow field measurements with that directly measured with a force balance. The collective evidence thus indicates that the 'non-circulatory' added mass force can be equally attributed to vorticity production in an otherwise inviscid flow field. The production of vorticity in a purely inviscid flow field is, however, something of a dilemma. Saffman[14] explained that changes to the vortex sheet are due to a topological change in the flow field, an effect which does not necessitate viscosity. Despite this, in a viscous flow field the vorticity would be generated in fluid elements immediate to the body walls and therefore could be experimentally measured in a real flow field. While, the effect of viscosity places vorticity into the flow field, for an unbounded flow the total impulse and thus force remains unchanged.[14] A series of experiments designed to measure the 'added mass vorticity production' are described next.

III. Experimental Methodology

PIV and flow visualisation experiments were performed on a flat plate wing undergoing linear acceleration at 90° incidence and an 'impulsively' angular accelerated flat plate rotated about the mid chord. Experiments were performed in a water towing tank on a wing model with a chord of 120 mm, thickness of 4 mm and a physical aspect ratio of 4. A skim plate was used on one end to give and effective aspect ratio of 8 due the mirror effect. All measurements considered hereafter were taken at the physical mid span of the plate.

A. PIV and dye flow setup

PIV measurements were taken using a commercial LaVision Flowmaster 2D PIV setup. A detailed description of the surging wing PIV setup can be found in Corkery et al.[3] For the rotation experiment titanium dioxide particles were illuminated using a Nd:YLF 527nm wavelength laser and photographed with a Phantom M310 camera at 200 Hz, and downsampled to 100 Hz. The camera field of view was centred tangential to the wing mid chord for both the rotating test case and for the first frame of the surge case. With the dual light sheet described in full by Stevens and Babinsky,[15] the setup enables the full flow field to be resolved without shadow regions. Vector fields for both experiments were determined by processing sequential frames with an initial interrogation window of 32x32 pixels for 2 passes, followed by a nominal 12x12 pixel deformable interrogation window with 2 passes and 50% overlap. Each PIV measurement presented is an ensemble average of 5 test runs. Dye flow visualisation was performed by injecting a milk-based dye mixture at points where flow is entrained into the shear layer leaving the sharp edges of the wing. For the surging experiment, the injection locations were approximately 4mm from the wing edge on the leeward face, while for the rotation experiments dye was injected on the advancing faces. For the rotating case the dye was illuminated with the dual laser light sheet described above, albeit with a defocussed beam width of approximately 20mm.

B. Wing kinematics

The kinematics for the surge and rotation cases are given in figures 7 and 8 respectively (also see corresponding schematics 5 and 6). For the surging profile the plate underwent constant acceleration over distance of 1 chord length, up to a Reynolds number of 10,000. Thereafter the plate traveled at constant velocity. For the rotation experiment, the plate was 'impulsively' rotated in the clockwise direction (angle defined by β and angular velocity Ω) from rest to a constant angular velocity (rotation frequency of 0.125 Hz) about an axis at the mid chord. At $\beta = 180°$ the plate is impulsively decelerated to rest.

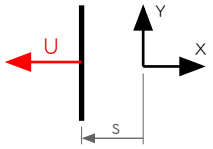

Figure 5: Surge schematic

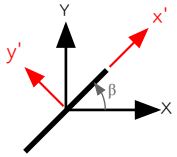

Figure 6: Rotation schematic

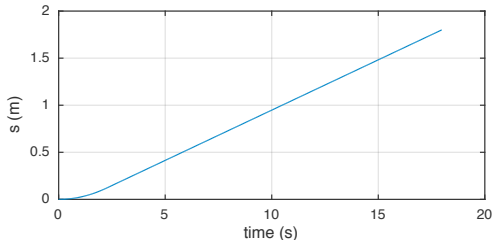

(a) Position

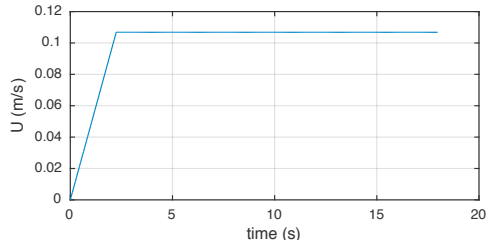

(b) Velocity

Figure 7: Surge kinematic profiles

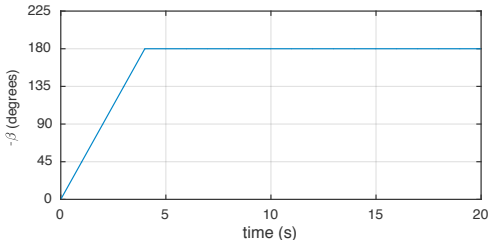

(a) Rotation angle

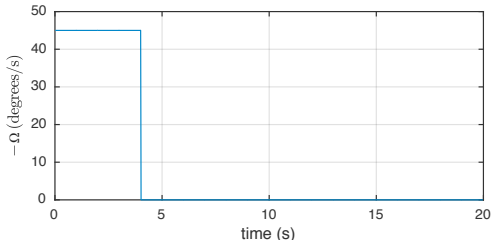

(b) Angular velocity

Figure 8: Rotation kinematic profiles

C. Vortex sheet measurement

A reliable method of measuring vorticity in the boundary layer of the plate was required to compare the physical flow field with that predicted by inviscid theory. While the strength of the boundary layer could in theory be directly measured from PIV measurements, the approach was not feasible here given both the limited spacial resolution of the PIV setup used, concerns of random error due to both laser reflections off the wing surface and partial obstruction of the particle plane close to the wing surface due to the camera and wing perspective. Secondly, even in a viscous flow field the boundary layer thickness for an impulsively accelerated body initially has zero thickness and thus equivalence with the Euler solution as diffusive effects have not had sufficient time to take effect. To avoid the aforementioned difficulties with direct boundary layer measurement, an alternative approach was developed.

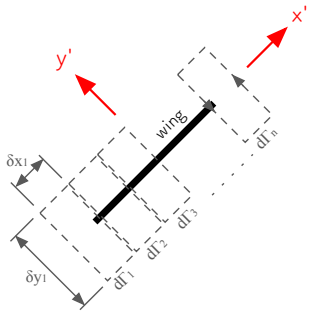

Figure 9: Schematic showing the discretisation of the flow field into a series of adjacent circulation elements.

First the plate and surrounding flow field was discretised into a series of adjacent rectangular elements as shown in figure 9. Circulation for each element was measured using the circular integral method ($d\Gamma = \oint u \cdot dl$), with fluid velocities at points adjacent to the known measurement values in the structured grid determined by linear interpolation. By application of Stokes' theorem (equation 11), each measurement of circulation using the circular integral method will automatically determine the vorticity in the boundary layers either side of the plate, as long as the boundary layer is within the closed line of integration.

$$\oint u \cdot dl = \int_A \omega dA \tag{11}$$

As the circulation contained in the boundary layer is equivalent to that of the inviscid vortex sheet, $\int_A \omega dA = \int \gamma dx'$, an estimation of the strength of the vortex sheet can be found by dividing the circulation of each element by the element width:

$$\gamma_n = d\Gamma_n / \delta x_n. \tag{12}$$

This method therefore allows the strength of the vortex sheet to be determined without requiring direct measurement of velocity gradients within the boundary layer on the plate. For the current experiment the plate was discretised into 50 area elements, over a distance of 1.5 chords in the x' direction ($\delta x = 0.03c$). Each element had a height of $\delta y = 0.30c$. The surge experiment had a relatively low acceleration rate, so to minimise noise a sequential average of the first 30 measurement frames of the scaled vortex sheet distribution is presented. This corresponds to a final plate displacement of 0.026 chords. The rotation experiment has a high angular acceleration, so a smaller sequential average of the first 5 frames was used. This corresponds to a final displacement of $\beta = 4.5°$.

IV. Results

A. Flow topology

Dye flow visualisation and PIV measurements for the surging plate is shown in figures 10 and 11, while figures 12 and 13 give the corresponding measurements for the rotating plate. The PIV measurements show normalised flow vorticity (red positive, blue negative) and quiver arrows with flow direction.

In the surging case the following can be observed:

- At $s/c \approx 0$ no vortices are visible in the flow field, yet PIV measurements show a region of negative vorticity at the top of the plate and positive below.
- At $s/c = 0.5$ a pair of counter rotating vortices behind the upper and lower wing edges are visible in both the dye flow and PIV measurement.
- At $s/c = 1.0$ the pair of vortices has moved downstream relative to the wing and a shear layer feeding the vortices can be seen. In the shear layer discrete blobs of dye are visible, which are the result of grouping of the shear layer into discrete vortices in the form of a Kelvin-Helmholtz vortex pattern.

For the rotating wing case the following can be observed:

- Similar to the surging case, at $\beta \approx 1°$ no vortices are visible in the flow field from dye flow visualisation, while positive vorticity is observed at the plate edges and negative around the centre from PIV.
- At $\beta = 90°$ a positive vortex has shed at each plate edge, which is fed by a visible shear layer. Again a Kelvin-Helmholtz instability is seen. A negative bound vortex sheet is visible toward the centre of the plate.
- At $\beta = 180°$ the pair of vortices has moved further downstream relative to the circumferential path of the plate edges. The Kelvin-Helmholtz instability is less coherent, however, this appears to be a result of secondary flow separation interacting with the primary shear layer. The secondary separation can be seen by the thickening of the negative bound vorticity toward the plate edges.

For both kinematic cases, at the start of motion no vortices are visible in the flow visualisation images, yet PIV measurements show finite vorticity distributed around the wing. In the following section this vorticity distribution will be compared with the equivalent potential flow solution if the wing were represented by a vortex sheet.

(a) s/c = 0

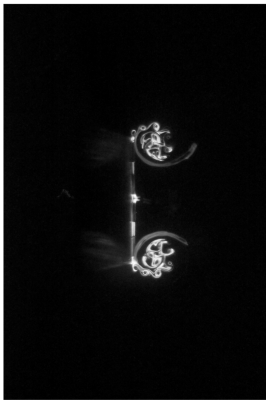

(b) s/c = 0.5

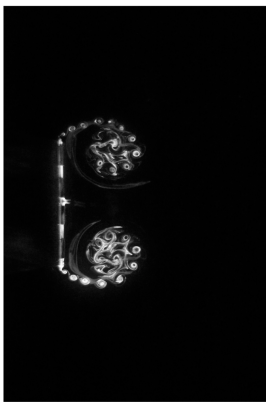

(c) s/c = 1.0

Figure 10: Dye flow visualisation for wing positions s/c = 0, 0.5 and 1.

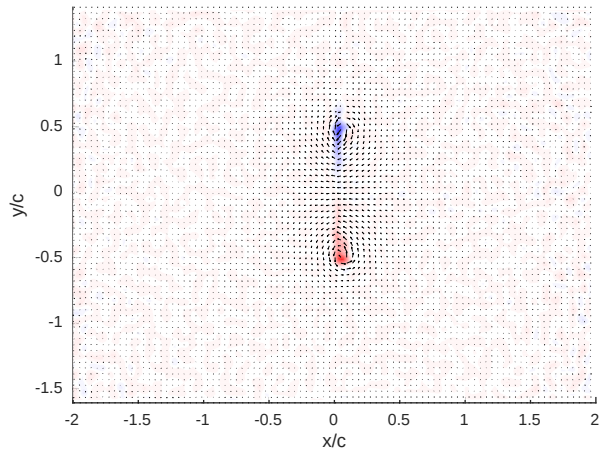

(a) s/c = 0.003

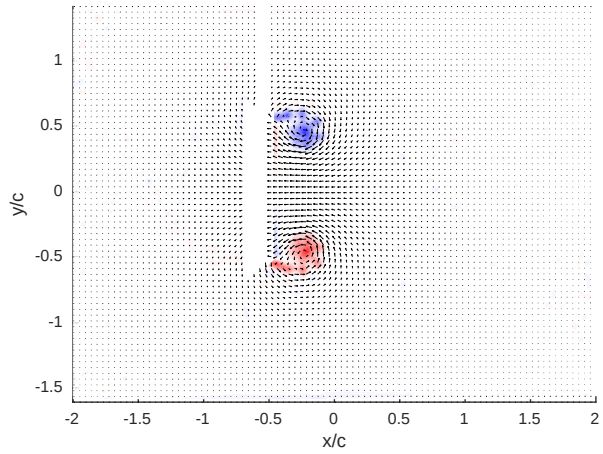

(b) s/c = 0.5

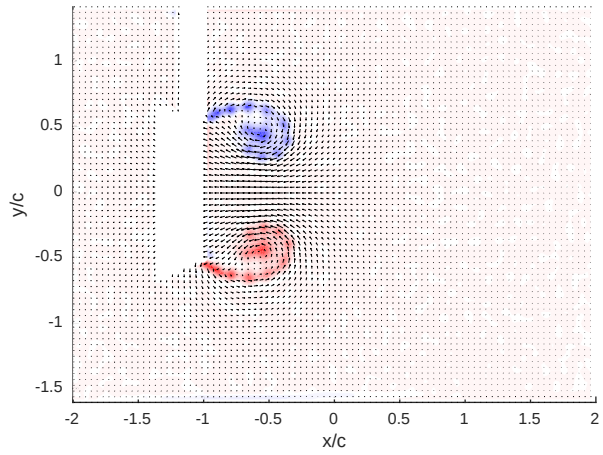

(c) s/c = 1.0

Figure 11: PIV measurements showing flow direction and normalised vorticity.

(a) $\beta \approx 1°$

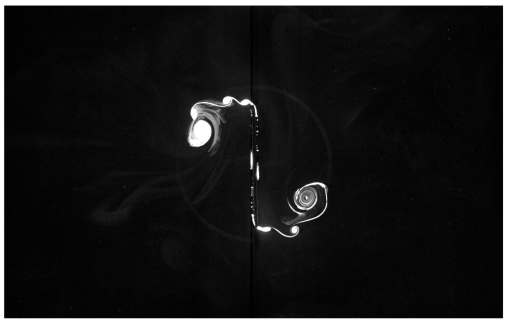

(b) $\beta = 90°$

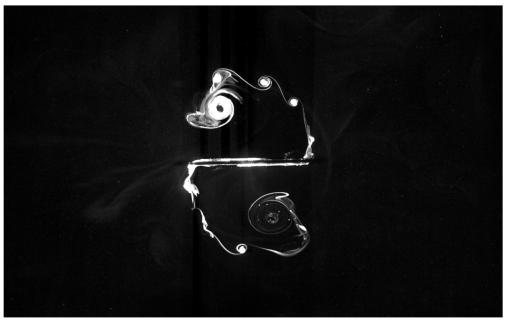

(c) $\beta = 180°$

Figure 12: Dye flow visualisation for rotation angles 1°, 90° and 180°.

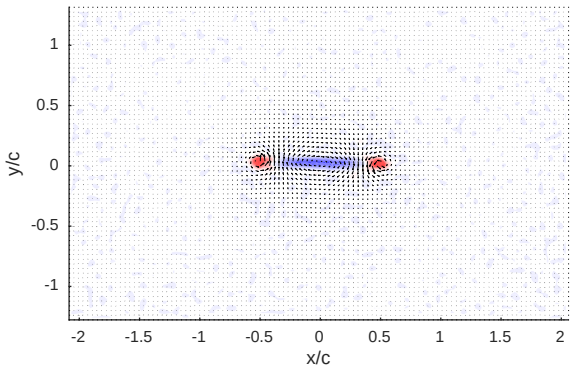

(a) $\beta \approx 1°$

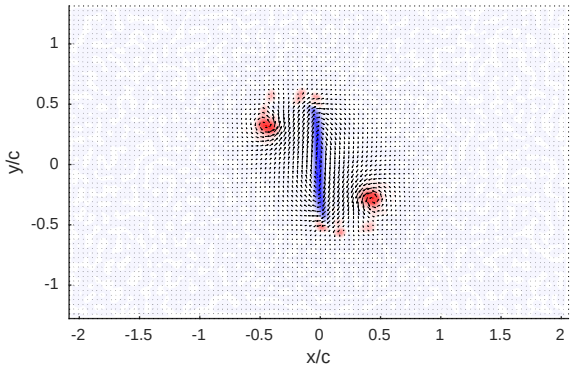

(b) $\beta = 90°$

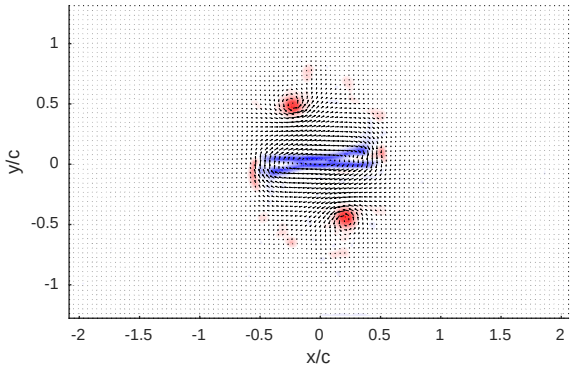

(c) $\beta = 180°$

Figure 13: PIV measurements showing flow direction and normalised vorticity.

B. Vortex sheet

The vortex sheet distributions as calculated from the PIV data shown in figures 11 and 13 is now considered for the start of the wing motion ($s/c \approx 0$ and $\beta \approx 0$). In figure 14a the measured and potential solutions for the surge case is compared, while figure 14b shows the rotational case. Each measurement has been scaled with the respective translational or angular velocities.

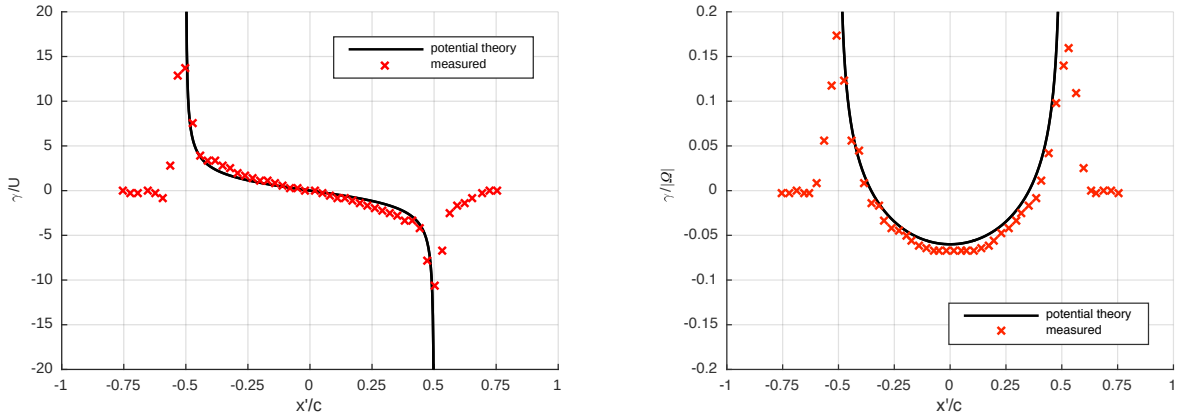

(a) Translation: $s/c \approx 0$

(b) Rotation: $\beta \approx 0°$

Figure 14: Comparison of measured and potential flow vortex sheets for a translating and rotating flat plate.

It can be seen that the measured vortex sheet closely matches the potential theory given by equation (10) for both the translation and rotational cases. Perhaps the most significant deviation between measurement and theory is toward the plate edges, whereby the theoretical sheet strength asymptotes toward infinity, whilst measurements form a sharp peak and drop toward zero beyond the plate edges. Given both the discretised method used to calculate the strength of the vortex sheet and the spacial averaging involved in vector calculation for PIV (each interrogation window has a nominal width of 0.04c), it is not possible to obtain the extremely high values.

Application of the Kutta condition could perhaps provide an alternative explanation as to why the measured vortex sheet varies from potential theory toward the plate edges. In steady flow streaming past a flat plate aerofoil, the Kutta condition ensures that there is zero pressure difference between the upper and lower surfaces at the trailing edge[11] and thus the strength of the vortex sheet here is zero due to equal flow velocities either side of the plate. The unsteady equivalent enforces the condition that the flow velocity and thus strength of the vortex sheet must be bounded, which can be satisfied through extension of the bound vortex sheet past the plate edges and into the flow field as a free vortex sheet.[16,17] At the plate edge the strength of the 'free' vortex sheet must be equal to the bound vortex sheet.[11] This seems somewhat logical, if the flow on one face of the plate is unable to travel around the plate edge due to flow separation, then by application of continuity it must continue past the plate edge. On the other face, flow must move toward the plate centre, which again would start from outside of the plate edges. The vortex sheet, equal to the discontinuity in flow velocity would therefore project past the wing edges and into the flow field in a continuous manner. Whether the variation between the measured vortex sheet and potential theory is physical, or just an artefact of the limitations of the used measurement methods, the effect appears to be minor compared to the overall distribution of the bound vortex sheet. This may likely however, have further secondary effects by varying the growth rate of free vortices in the flow field.

It was shown above that for nominally 'impulsive' and continually accelerating starting motions, the flow field is close to the potential solution and thus the distribution of vorticity generated in the boundary layer of the plate can be predicted. At this point the force on the plate is due to added mass, which therefore goes hand in hand with the growing vorticity field. While this was demonstrated for starting motion, it is also correct for a fully developed viscous flow field with separation. This is a flow field with significant

topological differences compared with the potential solution.

We will consider the region of impulsive deceleration for the rotating wing test case. Figure 15 shows the flow field before ($\beta = 180^-$) and after ($\beta = 180^+$) the deceleration impulse. The flow fields appear at first remarkably similar, however, there is a slight difference in the vorticity toward the surface of the plate.

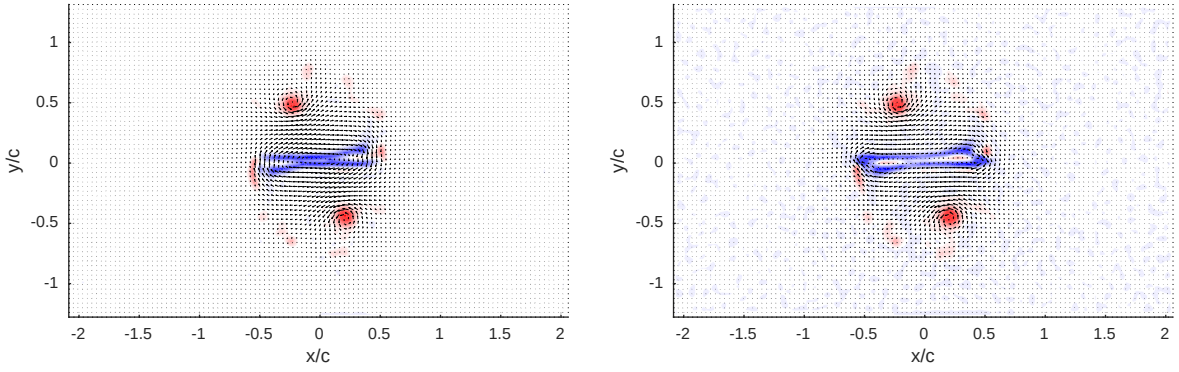

(a) $\beta = 180^-$ (b) $\beta = 180^+$

Figure 15: PIV measurements of the flow field before and after the deceleration impulse.

If the difference in the flow field is taken before and after the impulse we attain figure 16a. Immediately we see that the change in flow field is equivalent, albeit the inverse, to that produced during the starting motion shown previously in figure 13a. A measurement of the instantaneous change in distribution of the vortex sheet is shown in figure 16b. We find that the change in distribution is almost identical to that predicted by potential theory, albeit the measurements are slightly noisy and preserve the smearing of the vortex sheet past the plate edges.

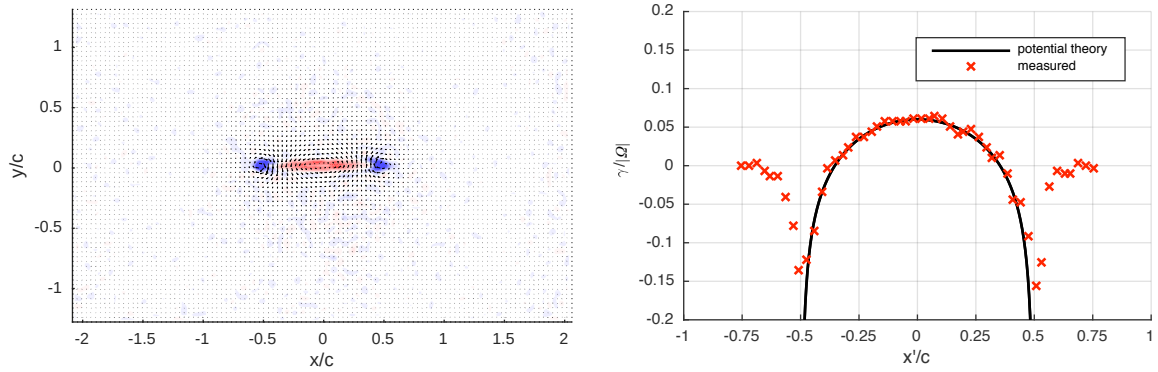

(a) Change in flow field (b) Change in vortex sheet

Figure 16: Change in vortex sheet over the impulsive deceleration at $\beta = 180°$.

The measurements thus show that even in a highly separated viscous flow field, that has significant topological differences to the inviscid potential solution, changes in the flow field due to acceleration is equivalent to that of inviscid potential flow (aside from the uncertainty surrounding the edge condition). The evidence thus suggests that the change in force on the plate (or flow field), is equivalent to the potential solution for all flows, whether that be inviscid and attached, or a fully developed viscous flow with significant separation.

V. Conclusions

The aims of this paper were to discuss mechanisms that contribute to force production for flat plate wings. A flat plate wing was accelerated in both a linear and rotational manner in a towing tank and changes to the flow field were qualitatively determined with aid of flow visualisation and quantified with PIV measurement. The following conclusions can be made:

- A flat plate wing, which is often modelled by an 'inviscid vortex sheet' can be deconstructed into components attributed to translation, rotation and external vortices.
- The forces due to added mass, in both the translation and rotational sense can be explained by a change in strength of the inviscid vortex sheet. This is equivalent to the production of vorticity in the boundary layer for a physical viscous flow field.
- PIV measurements of elemental areas encompassing the plate can be used to determine the distribution of vorticity in the boundary layer, without requiring velocity gradients within the boundary layer to be directly resolved.
- Good agreement between experiment and potential theory of the vortex sheet was shown.
- It was shown experimentally that the production of vorticity due to added mass and therefore the force due to change in impulse is independent of flow topology.
- The distribution of 'added mass vorticity' appears independent of viscous effects, albeit with a possible exception at the plate edges.

References

[1]Bisplinghoff, R. L., Ashley, H., and Halfman, R. L., *Aeroelasticity*, Addison-Wesley series in mechanics, Addison-Wesley, Cambridge, MA, 1955.

[2]Ol, M. and Babinsky, H., "Extensions of Fundamental Flow Physics to Practical MAV Aerodynamics: TR-AVT-202," Tech. rep., North Atlantic Treaty Organization, 2016.

[3]Corkery, S. J., Stevens, P. R. R. J., and Babinsky, H., "Low Reynolds Number Surge Response of a Flat Plate Wing at 90 Degrees Incidence," *AIAA SciTech Forum - 55th AIAA Aerospace Sciences Meeting*, 2017, pp. 1–16.

[4]Milne-Thomson, L. M., *Theoretical Hydrodynamics*, Macmillan, 5th ed., 1986.

[5]Eldredge, J. D. and Wang, C., "High-fidelity simulations and low-order modeling of a rapidly pitching plate," *AIAA Paper*, , No. July, 2010, pp. 1–19.

[6]Michelin, S. and Llewellyn Smith, S. G., "An unsteady point vortex method for coupled fluid-solid problems," *Theoretical and Computational Fluid Dynamics*, Vol. 23, No. 2, 2009, pp. 127–153.

[7]Babinsky, H., Stevens, P. R. R. J., Jones, A. R., Bernal, L. P., and Ol, M. V., "Low Order Modelling of Lift Forces for Unsteady Pitching and Surging Wings." *54th AIAA Aerospace Sciences Meeting*, jan 2016, pp. 1–12.

[8]Lamb, H., *Hydrodynamics*, Cambridge University press, 1895.

[9]Pitt Ford, C. W., *Unsteady aerodynamic forces on accelerating wings at low Reynolds numbers.*, Ph.D. thesis, The University of Cambridge, 2013.

[10]Wu, J. C., "Theory for Aerodynamic Force and Moment in Viscous Flows," *AIAA Journal*, Vol. 19, No. 4, apr 1981, pp. 432–441.

[11]Xia, X. and Mohseni, K., "Unsteady Aerodynamics and Vortex-sheet Formation of A Two-dimensional Airfoil," *Journal of Fluid Mechanics*, Vol. 830, 2016, pp. 439–478.

[12]Manar, F. and Jones, A. R., "Vorticity Production at the Leading Edge of Flat Plates at High Incidence," *AIAA SciTech Forum - 55th AIAA Aerospace Sciences Meeting*, No. January, Grapevine, Texas, 2017, pp. 1–11.

[13]Graham, W. R., Pitt Ford, C. W., and Babinsky, H., "An impulse-based approach to estimating forces in unsteady flow," *Journal of Fluid Mechanics*, Vol. 815, 2017, pp. 60–76.

[14]Saffman, P. G., *Vortex Dynamics*, Cambridge University Press, 1992.

[15]Stevens, P. R. R. J. and Babinsky, H., "Experiments to investigate lift production mechanisms on pitching flat plates," *Experiments in Fluids*, Vol. 58, No. 1, 2017, pp. 7.

[16]Pullin, D. I., "The large-scale structure of unsteady self-similar rolled-up vortex sheets," *Journal of Fluid Mechanics*, Vol. 88, No. 03, 1978, pp. 401.

[17]Pullin, D. I. and Perry, A. E., "Some flow visualization experiments on the starting vortex," *Journal of Fluid Mechanics*, Vol. 97, No. 2, 1980, pp. 239–255.